J. Synchrotron Rad. (1999). **6**, 379–380

Polarized Ni *K*- and *L*-edge and S *K*-edge XANES study of $[Ni(III)(mnt)_2]^{1-}$

Takaki Hatsui, Yasutaka Takata, Nobuhiro Kosugi

[a]The Graduate University for Advanced Studies, Institute for Molecular Science, Myodaiji, Okazaki 444-8585, Japan
Email:kosugi@ims.ac.jp

In order to characterize the singly occupied molecular orbital (SOMO) of $[(C_2H_5)_4N][Ni^{III}(mnt)_2]$ (mnt: 1,2-dicyanovinylene-1,2-dithiolato), polarized XANES spectra are investigated at the Ni *K*-edge, Ni *L*-edge, and S *K*-edge. Two weak Ni $1s \rightarrow 3d^*$ and two strong Ni $2p \rightarrow 3d^*$ transitions are observed, and the lower peak in energy is assigned to the transitions to SOMO. The polarization dependence of the lower peak revealed that SOMO has the b_{2g} symmetry with out-of-plane $3d_{xz}\pi^*$ character. The transition to SOMO is also found in the S *K*-edge XANES, indicating significant ligand π^* contribution in SOMO.

Keywords: Ni 1,2-dithiolene complex, trivalent Ni, SOMO, polarized XANES

1. Introduction

The X-ray absorption near edge structure (XANES) is useful to characterize unoccupied states, and comparison of the XANES spectra at different absorption edges is essential to determine symmetries and atomic components of the unoccupied states. Furthermore, polarized XANES measurement is very important to reveal the symmetries in detail. Thus, the XANES has been widely used to study what hole is created in high-Tc superconducting cupurate compounds (for example, Kosugi *et al.*, 1989, 1990).

The XANES is applicable to study the character of holes created in organic semiconductors and conductors. In the present work, polarized XANES spectra at different absorption edges are investigated to reveal the electronic structure of an organic semiconductor with a formally trivalent Ni metal, $[(C_2H_5)_4N][Ni^{III}(mnt)_2]$ (mnt: 1,2-dicyanovinylene-1,2-dithiolato). In this system, it is believed that the mnt ligands are partially oxidised and the Ni metals have oxidation numbers between 2 and 3 (Kobayashi & Sasaki, 1977; Kobayashi & Kobayashi, 1997). However, discussion on the Ni valency is still controversial in X-ray photoelectron spectroscopy (XPS) (Matienzo *et al.*, 1973; Grim *et al.*, 1974; Sano *et al.*, 1981; Lalitha *et al.*, 1988). We expect that a conclusive discussion on the Ni valency will be possible based on the XANES. The present authors have revealed the electronic structure of the $[(n\text{-}C_4H_5)_4N]_2[Ni^{II}(mnt)_2]$ system with a formally $3d^8$ low-spin Ni configuration (Hatsui *et al.*, 1999). Our concern in the present work is what kind of orbital has a single hole in $[Ni^{III}(mnt)_2]^{1-}$ in comparison with $[Ni^{II}(mnt)_2]^{2-}$.

Ni *K*-edge XANES spectra were measured in transmission mode at BL-10B of the Photon Factory. Ni *L*-edge and S *K*-edge XANES spectra were measured by total electron yields at the soft X-ray double crystal monochromator beamline BL1A of the UVSOR facility. A single crystal of $[(C_2H_5)_4N][Ni(mnt)_2]$ was obtained by the published method (Kobayashi *et al.*, 1977).

2. Results and discussions

2.1. Polarized Ni K-edge XANES of $[Ni^{III}(mnt)_2]^{1-}$

Figure 1 shows polarized Ni *K*-edge XANES spectra of $[(C_2H_5)_4N][Ni^{III}(mnt)_2]$. The molecular geometry of $[Ni^{III}(mnt)_2]^{1-}$ ion has nearly D_{2h} symmetry (Kobayashi *et al.*, 1977) as inserted in Fig. 1. The spectral feature and polarization dependence observed are very similar to those of $[(n\text{-}C_4H_5)_4N]_2[Ni^{II}(mnt)_2]$ (Hatsui *et al.*, 1999), except for a new extra feature X at the $1s$-$3d$ region in the E//z spectrum. Weak feature X is about 0.4 eV lower in energy than feature A. A similar extra feature at the $1s$-$3d$ region is observed in $K_3Fe^{III}(CN)_6$ in comparison with $K_4Fe^{II}(CN)_6{\cdot}3H_2O$ (Kosugi *et al.*, 1986). This indicates that $[Ni^{III}(mnt)_2]^{1-}$ has a singly occupied molecular orbital (SOMO) with $3d$ character, which is doubly occupied in $[Ni^{II}(mnt)_2]^{2-}$. Observation of extra feature X with the lowest energy is consistent with the higher oxidation number of Ni atom in $[Ni^{III}(mnt)_2]^{1-}$ than in $[Ni^{II}(mnt)_2]^{2-}$. Feature A is observed in the (E//x, k//y) and (E//y, k//x) spectra and is undoubtedly assigned to a quadrupole transition to Ni $3d_{xy}^*(b_{1g}^*)$. Feature b is observed in the E//z spectrum and is assigned to a dipole-allowed Ni $1s \rightarrow 4p\pi^*$ transition with no large metal-to-ligand charge transfer (MLCT) character, because of the absence of low-lying $b_{1u}^*(L_z^*)$ ligand orbitals combined with Ni $4p\pi^*$ orbital (Hatsui *et al.*, 1999). On the other hand, weak features c and d are observed in the E//y and E//x spectra, respectively, and are assigned to MLCT transitions to the in-plane CN π^* (b_{2u}^*, L_y^*) and CN σ^* (b_{3u}^*, L_x^*) orbitals (Hatsui *et al.*, 1999).

2.2. Polarized Ni L-edge XANES of $[Ni^{III}(mnt)_2]^{1-}$

Figure 2 shows polarized Ni *L*-edge XANES of $[Ni^{III}(mnt)_2]^{1-}$. The spectral feature and polarization dependence observed are very similar to those of $[(n\text{-}C_4H_5)_4N]_2[Ni^{II}(mnt)_2]$ (Hatsui *et al.*, 1999), except for observation of a new extra feature X which is

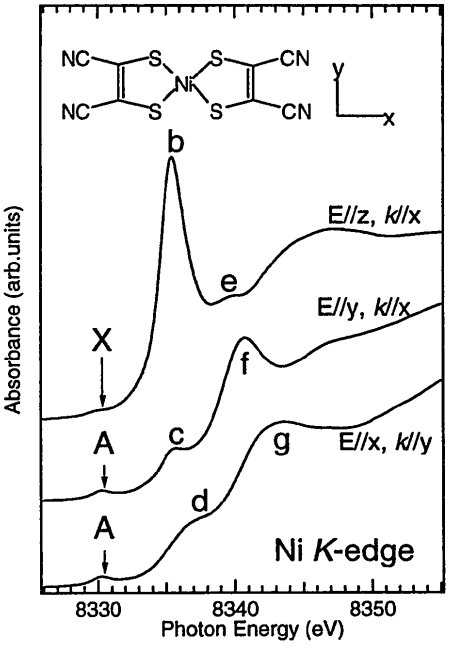

Figure 1
Polarized Ni *K*-edge XANES spectra of $[(C_2H_5)_4N][Ni^{III}(mnt)_2]$, where E and k denote the electric vector and wave vector of incident light, respectively. The molecular geometry of $[Ni^{III}(mnt)_2]^{1-}$ ion is shown as inset.

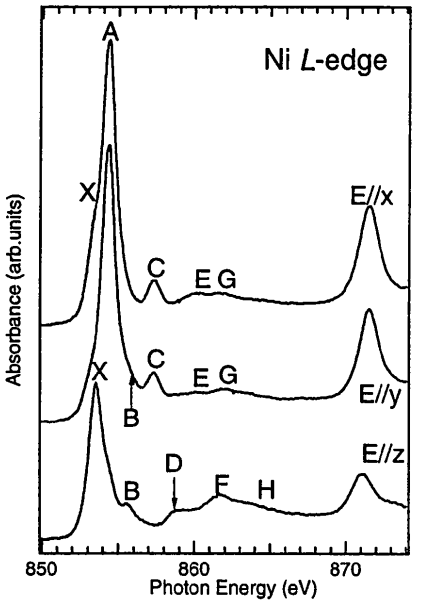

Figure 3
Polarized Ni L-edge XANES spectra of $[(C_2H_5)_4N][Ni^{III}(mnt)_2]$, where E denote the electric vector of incident light.

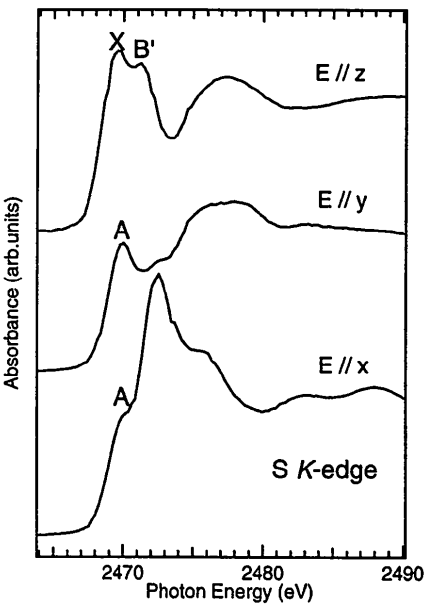

Figure 3
Polarized S *K*-edge XANES spectra of $[(C_2H_5)_4N][Ni^{III}(mnt)_2]$, where E denote the electric vector of incident light.

0.8 eV lower in energy than feature A. Feature X is observed predominately in the E//x and E//z spectra and feature A is observed predominately in the E//x and E//y spectra, though $[Ni^{III}(mnt)_2]^{1-}$ ions are not completely parallel to one another in the single crystal. As feature A is assigned to the transition to Ni $3d_{xy}$*(b_{1g}*) with antibonding character with ligand orbitals, feature X is also assigned to the transition to Ni $3d_{xz}$*(b_{2g}*) with antibonding character with ligand orbitals; that is, the symmetry of SOMO is b_{2g}*. Considering that the intensity ratio X/A is estimated to be about 0.3 (less than 0.5) for the non-polarized spectrum, the ligand contribution is larger in the b_{2g}*($3d_{xz}$*) orbital than in the b_{1g}*($3d_{xy}$*) orbital. On the other hand, feature B is very weak in the E//x spectrum and feature C is not observed in the E//z spectrum; features B and C are assigned to MLCT transitions to low-lying unoccupied ligand orbitals with b_{3g}*(L_{yz}*) and a_g*(L_{x2-y2}*) symmetries, respectively (Hatsui *et al.*, 1999).

2.3. Polarized S K-edge XANES of $[Ni^{III}(mnt)_2]^{1-}$

Figure 3 shows polarized S *K*-edge XANES spectra of $[Ni^{III}(mnt)_2]^{1-}$. Feature X is not observed in the spectra of $[Ni^{II}(mnt)_2]^{2-}$. Other features are similarly observed in $[Ni^{II}(mnt)_2]^{2-}$. Feature X is observed in the E//z spectrum, indicating π* character. This is consistent with the b_{2g} symmetry of the SOMO. The highest occupied molecular orbital (HOMO) with $5b_{2g}$ symmetry in $[Ni^{II}(mnt)_2]^{2-}$ is delocalized over Ni atom and ligands, as illustrated in Figure 4. This orbital should correspond to SOMO in $[Ni^{III}(mnt)_2]^{1-}$. Features A is observed in the E//x and E//y spectra and feature B' is observed in the E//z. This is consistent with the Ni *L*-edge features; that is, features A is assigned to b_{1g}*($3d_{xy}$*). A ligand $[(mnt)_2]^{4-}$ has a low-lying out-of-plane ligand π* orbital, which produces b_{3g}*(L_{yz}*) orbital and a ligand orbital with a_u* symmetry in $[Ni^{III}(mnt)_2]^{1-}$. They are expected to be close in energy and attributable to feature B'.

The authors acknowledge valuable advice on the sample preparation by Dr. Hideki Fujiwara and kind support for the measurement of X-ray diffraction by Dr. Masaaki Tomura.

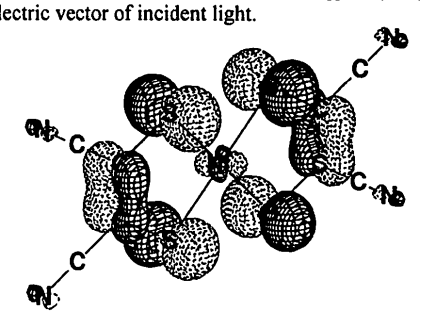

Figure 4
Illustration of HOMO ($5b_{2g}$) for $[Ni^{II}(mnt)_2]^{2-}$.

References

Grim, S.O., Matienzo, L.J., Swartz Jr., W.E. (1974). *Inorg. Chem.* **13**(2), 447-449.

Hatsui, T., Takata, Y., Kosugi, N. (1998). *Chem. Phys. Lett.* **284**, 320-324.

Hatsui, T., Takata, Y., Kosugi, N. (1999). To be published in this volume.

Kobayashi, A. & Kobayashi, H. (1997). in *Handbook of Organic Conductive Molecules and Polymers*, Vol. 1, edited by H.S. Nalwa, pp. 249-291, Chichester: John Wiley & Sons.

Kobayashi, A., Sasaki, Y. (1977). *Bull. Chem. Soc. Jpn.* **50**(10), 2650-2656.

Kosugi, N., Yokoyama, T., Kuroda, H. (1986). *Chem. Phys.* **104**, 449-453.

Kosugi, N., Kondoh, H., Tajima, H., Kuroda, H. (1989). *Chem. Phys.* **135**, 149-160.

Kosugi, N., Tokura, Y., Takagi, H., Uchida, S. (1990). *Phys. Rev.* **B41**(1), 131-137.

Lalitha,S., Chandramouli, G.V.R., Manoharan, P.T. (1988). *Inorg. Chem.* **27**(8), 1492-1498.

Matienzo, L.J., Yin, L.I., Grim, S.O., Swartz Jr., W.E. (1973). *Inorg. Chem.* **12**(12), 2762-2769.

Sano, M., Adachi, H., Yamatera, H. (1981). *Bull. Chem. Soc. Jpn.* **54**(9), 2636-2641.

(Received 10 August 1998; accepted 29 January 1999)